Modern Environmental Science and Engineering (ISSN 2333-2581)
June 2020, Volume 6, No. 6, pp. 625-644
Doi: 10.15341/mese(2333-2581)/06.06.2020/001
Academic Star Publishing Company, 2020
www.academicstar.us

Post-Scan Georeferencing of LiDAR Data from a Geological Exposure using ArcGIS™ for Adjustment

Trevor B. Kelly[1], Grant D. Wach[1], and Darragh E. O'Connor[1, 2]

1. Department of Earth and Environmental Sciences, Dalhousie University, Halifax, Canada

2. Department of Earth and Environmental Sciences, University of Manchester, Manchester, United Kingdom

Abstract: With the commonality of LiDAR increasing in usage amongst a wide array of disciplines, questions will arise regarding how the data is to be used and with what software the data will be visualized, manipulated, and utilized. One question that arises is whether a georeferenced point cloud is required and if so, should direct georeferencing be performed during a LiDAR scan or completed post-scan. Georeferencing, in terms of LiDAR, is the process in which real-world coordinates are assigned to every point in the point cloud such that all data points are grounded where they would be on earth. LiDAR scans don't need to be georeferenced; however, for many geological studies, it is particularly important, especially when other types of data are to be integrated. Overall, this can lead to improved geological interpretations. For geological outcrops, such as the cliff face exposed at Joggins, Nova Scotia, the need for georeferenced LiDAR scans is essential for research relating to the density of the fossilized forest for paleo-reconstruction studies, for reservoir heterogeneity, compartmentalization studies, fluvial channel body aspect ratios, or the erosion rate of the cliff face. To save time at the geological exposure, georeferencing is not performed directly by the LiDAR system, but rather the coordinates from three strategically placed control points were recorded for post-scan georeferencing. This paper will introduce a workflow detailing the steps to achieve a fully georeferenced point cloud by knowing the ground locations of three targets incorporated into the LiDAR scan using conventional software, in this case, ArcGIS™.

Key words: LiDAR, remote sensing, georeferencing, workflow, point cloud

1. Introduction

Light Detection and Ranging (LiDAR) is used for a variety of applications, including, but not limited to scientific research [1-4], law enforcement [5-7], surveying [8, 9], and construction [10-12]. Current papers published on the topic of georeferencing tend to deal more with the application of mathematical concepts and equipment setup, rather than providing a procedural technique for achieving a georeferenced data set [13-20].

Despite the wide range of uses and different configurations among different disciplines, the premise of operation is similar; a laser pulse is emitted from the unit, travels to some remote target, reflects/refracts off the target, and returns to the detector [21]. The two-way travel time (source to target and target to detector) is halved and multiplied by the speed of light to obtain the Z distance. The X and Y positions are determined based on the location of the laser emitter when the pulse exits the instrument [21]. In addition to measuring the X, Y, and Z locations of thousands of pints per second, the LiDAR instrument also has the capability of measuring the laser/light intensity (I) at each X, Y, and Z location.

In the geoscience discipline, LiDAR has been a valuable tool for capturing 3D outcrops in point cloud form, from which very detailed sedimentological and stratigraphic interpretations can be carried out. It has been recognized that the resulting intensity values recorded by the LiDAR unit correlate extremely well to

Corresponding author: Trevor B. Kelly, Ph.D. Candidate; research areas/interests: earth and environmental sciences. E-mail: tbkelly@dal.ca.

lithology (Fig. 1), thereby allowing for the determination between sandstone and shale, for example [22, 23]. In many instances, it is essential to have a point cloud that is fully georeferenced, which is to say that the points in the point cloud have the same easting, northing, and elevation as they would on earth, instead of being in some generic X, Y, and Z space. For the scans that are performed by researchers of the Dalhousie University Basin and Reservoir Laboratory, the georeferencing of point clouds is carried out post-scan using georeferencing targets, as opposed to direct georeferencing performed during the scan. For this to be successful, three targets (control points) are placed at varying X, Y, and Z locations within the scan zone. The locations of these targets are measured and recorded using a real-time kinematic (RTK) differential global positioning system (DGPS). This helps to alleviate the main disadvantages of direct georeferencing, which are the increased time and precision required for instrument setup [17]. Moreover, post-scan georeferencing is particularly useful when the laser scanner does not have built-in GPS capabilities or the built-in GPS capabilities of the laser scanner is not well known, or when there could be potential errors in collecting GPS data directly during the scan, and for multiple scans that will be eventually merged, highly accurate RTK DGPS data is required, which laser scanners do not have as a built-in option.

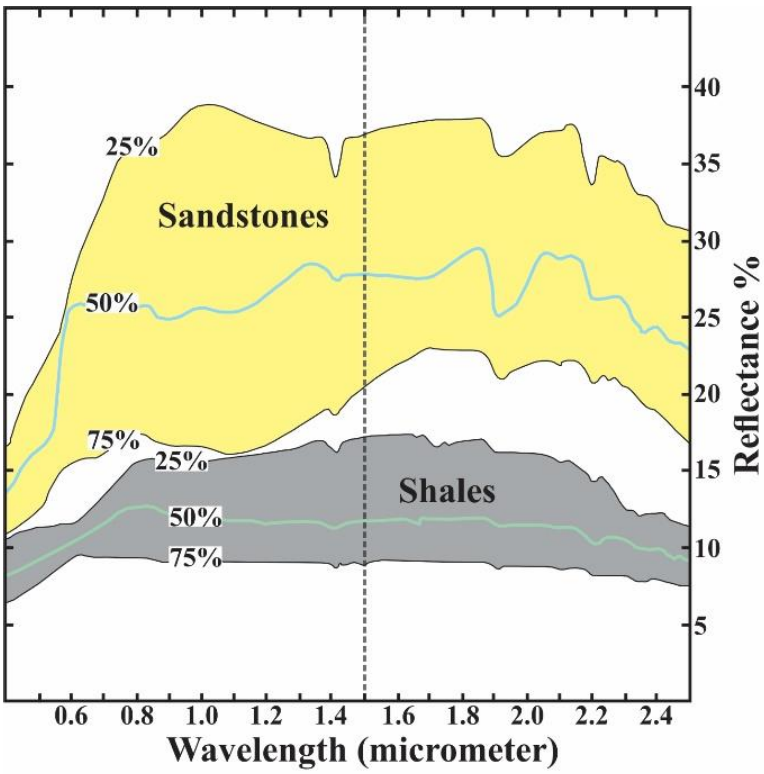

Fig. 1 A NASA JPL library spectroscopy solid sample data with the median (solid green line) and quartiles for shale (grey) and sandstone (yellow) [22, 23]. The dashed line at 1.5 micrometers is the approximate wavelength of terrestrial LiDAR. At the wavelength of terrestrial LiDAR, sandstone and shale have a noticeable spectral separability between them [23].

The purpose of this technical paper is to introduce a procedure by which georeferencing of point cloud data can be performed using standard and widely available programs and software. The workflow from raw point cloud data to a fully georeferenced data set is broadly divided into four parts: (1) data preparation, (2) creation of point cloud/georeferencing targets shapefiles, (3) point decimation, and (4) point cloud adjustment. This paper will make use of a data set collected in May of 2013 from the Joggins Formation located in the community of Joggins, Nova Scotia.

A fully georeferenced data set allows for a variety of studies, and detailed interpretations can be achieved, such as the determination of coastal erosion rates using multiple georeferenced scans performed over a length of time. Also, the Joggins Formation contains upright, fossilized trees, which is a characteristic that is unique to this site. The use of successive and georeferenced LiDAR scans could potentially give researchers the ability to determine the density of the paleo forest that once existed (Fig. 2). Moreover, a georeferenced point cloud can be easily integrated with other data gathering techniques, such as a ground-penetrating radar survey, for example.

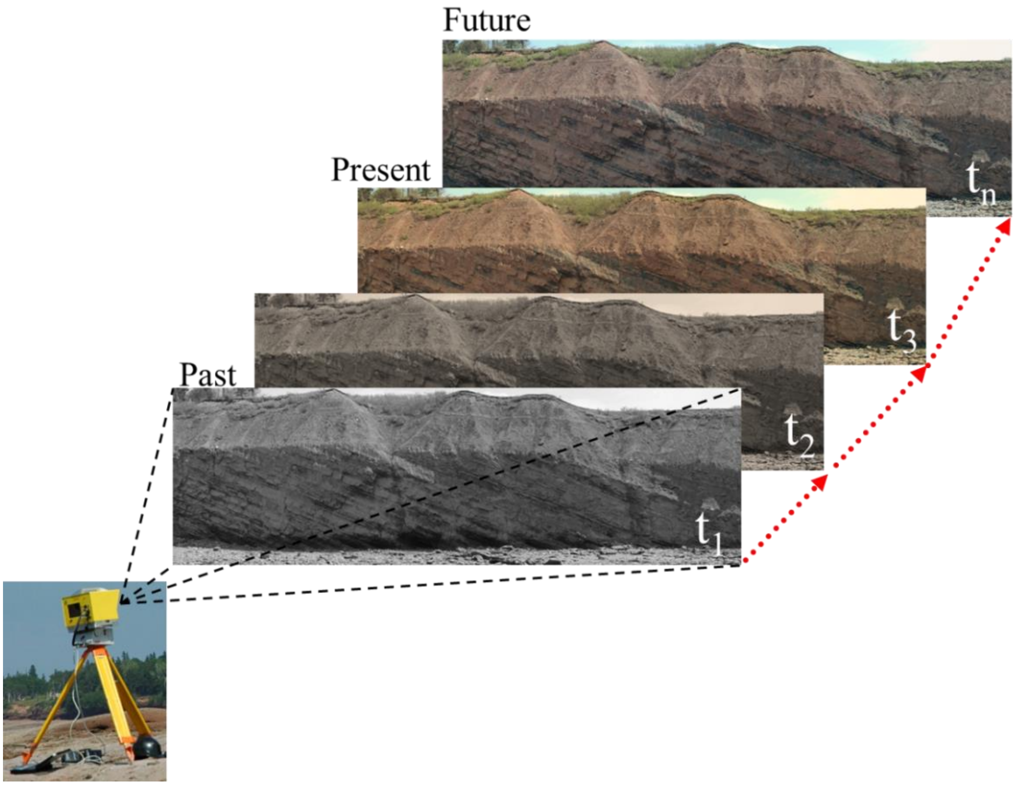

Fig. 2 Using successive, georeferenced LiDAR point clouds over some time, a variety of studies could potentially be completed [24]. These may relate to the paleo forest density or erosion studies.

1.1 Previous Work

The use of LiDAR in outcrop geology is not a recent trend; however, a search for LiDAR georeferencing-related outcrop papers does not yield many examples. For that reason, this paper is written out of the need for georeferencing ground-based, static LiDAR scans using accurate target locations for point cloud adjustment. An article by Schuhmacher and Böhm (2005) [18] deals with the subjects of sensor- and data-related georeferencing methods. In this paper, seven methods are tested in two separate experiments with the results showing the total accuracy for each method, with the conventional total station setup being the most accurate [18].

Habib et al. (2008) [13] perform a comparative, indirect georeferencing analysis in which three sources of control data are investigated; 1) ground control points, 2) LiDAR patches, and 3) LiDAR lines. A new method for the absolute orientation of a LiDAR point cloud was introduced by Mohamed and Wilkinson (2009) [15], in which they placed two antennas on top of a static LiDAR unit to provide higher data gathering precision for attitude determination. Field survey methods were introduced by Olsen et al. (2009) [16] as ways of georeferencing terrestrial LiDAR scans completed in a dynamic environment over a significant scan area distance. Wilkinson et al. (2010) [19] present a novel method that utilizes two firmly mounted antennas installed on the optical head of the LiDAR scanner to determine the absolute positioning of LiDAR point clouds.

A paper by Llorens et al. (2011) [14] shows how georeferenced information from LiDAR sensors can have potential benefits for crop management. In their research, they propose a workflow for obtaining a georeferenced canopy map from LiDAR and paring it with GPS data from a receiver installed atop a tractor. Olsen et al. (2011) [25] discuss the use of a new georeferencing technique with related algorithms for automating 3D point cloud georeferencing of large-scale scans. Zhang and Shen (2013) [20] identify and demonstrate the significant direct georeferencing distortion factors, such as the datum distortion scale and the earth curvature distortion and apply high-precision map projection correction formulas to airborne LiDAR data for direct georeferencing. While these papers are useful for determining such things as the optimum equipment setup that will lead to the most accurate data set, they do not present much in the form of a workflow for taking raw data with an arbitrary coordinate system and converting into data that has real-world coordinates.

The Joggins Formation itself has been studied for over 150 years [26]. The majority of the research conducted in this area can be grouped into three all-encompassing categories. The first being geology (e.g., sedimentology and stratigraphy); the second being paleobiology (e.g., discovery and taxonomy); and the third being paleoenvironmental reconstructions that incorporate the previous two categories [26]. Grey and Finkel (2011) [26] summarize the bulk of the research within the three categories mentioned above from past to present and provide insight for future work that could arise.

1.2 Study Area

The location of the study area is approximately 230 km north of Halifax, Nova Scotia, in the village of Joggins on the coastline of Chignecto Bay, an inlet of the Bay of Fundy where the tides ebb and flow some 13 meters twice daily (Fig. 3A). This area was selected due to the continuity and quality of the 2D exposure of the outcrop known as the Joggins Formation, in addition to the ease of access. The section of the scanned outcrop is located just north of Coal Mine Point (Fig. 3B), which is a sandstone headland composed of more resistant, less erosive rock that displays a significant change in depositional style that is still discussed and debated. The Joggins Fossil Cliffs (Joggins Formation) along with six other conformable formations (Ragged Reef, Springhill Mines, Little River, Boss Point, Claremont, and Shepody) were designated in 2008 as a United Nations Educational, Scientific and Cultural Organization (UNESCO) heritage site, because of the beautifully exposed and preserved rock layers demonstrating the most complete and comprehensive fossil record of life during the "Coal Age", a period when lush forests and swamps occurred over much of the World's tropics [27].

Joggins and the surrounding area have an extensive history of coal mining, dating back to 1686 and continuing for over 200 years [28]. Intricate underground mine workings were established, with some of the remnants (e.g., mine openings and support timbers) visible within the cliff face. There is also evidence of some of the topside development relating to coal mining in the form of timbers (rail track and support) and steel spikes on the beach between Main Street and the Joggins Fossil Cliffs Centre and remains of a wooden pier that existed for loading coal onto ships during high tide for destinations throughout the Maritimes and New England [28]. The section of the Joggins Formation chosen for scanning does not show evidence of any historical coal mine workings.

2. Equipment and Methods

2.1 Terrestrial Laser Scanning

Stationary ground-based laser scanning was achieved by using the tripod-mounted Dalhousie

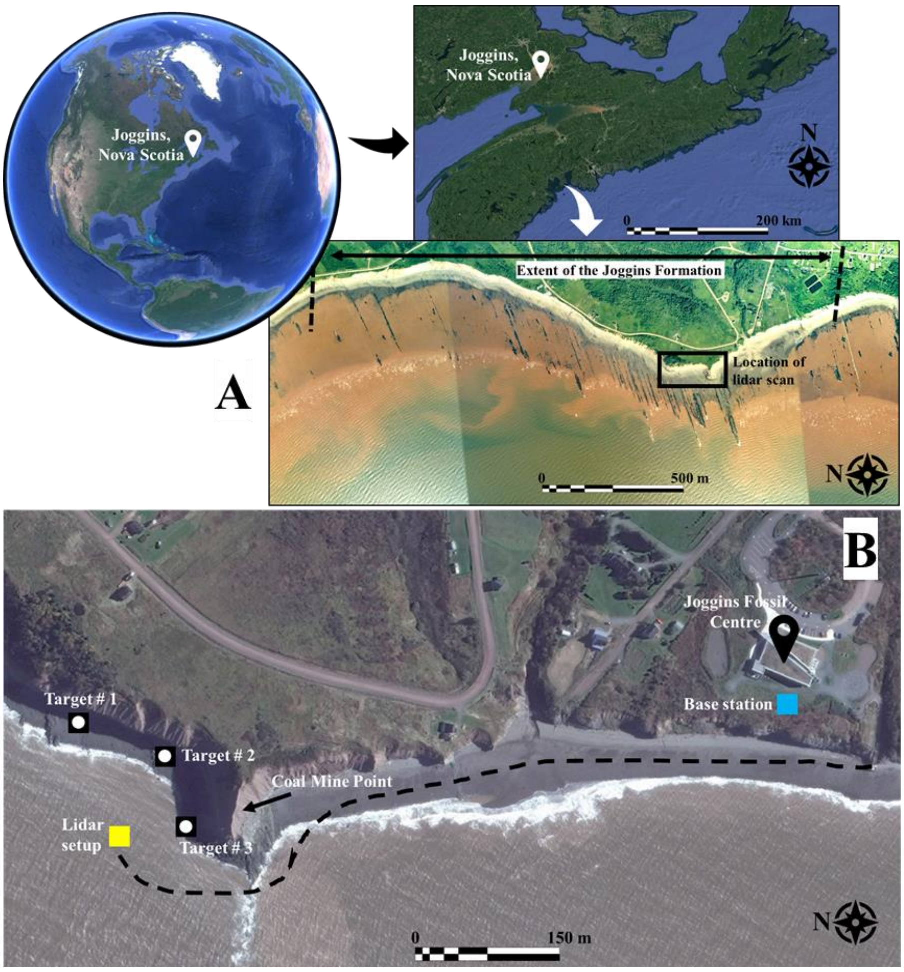

Fig. 3 A) Location map of Joggins, Nova Scotia. The zoomed-in aerial photograph is annotated to show the extent of the Joggins Formation and the location of the LiDAR scan [29, 30]. B) Aerial photograph of various points of interest. The Joggins Fossil Centre is located near the top right. The blue box just to the south of the centre is the location of the base station. The black dashed line indicates the route that was taken to reach the Coal Mine Point scan area. The LiDAR setup is indicated by the yellow box in the lower left-hand quadrant of the photograph with the locations of the three target setups shown by a black box with a white circle in the middle.

University Basin and Reservoir Laboratory Optech Incorporated Intelligent Laser Ranging and Imaging System (ILRIS) 3D LiDAR scanner (Fig. 4) with a scan speed of 2.5 kHz and 2,500 points per second [31]. LiDAR is an exceedingly versatile ground-, air-, and water-based instrument for the remote collection of data and it has been employed comprehensively to an array of disciplines including geoscience [3, 21, 32-37]. LiDAR scanning bombards a surface (in this case, a rock face) with pulsating laser energy and measures the difference in time between the primary pulse emission and the returning signal detection. The emitted laser pulse has a wavelength of 1,535 nm (infrared spectrum). To obtain a reflection, the rock being inundated by laser pulses must be of the type to produce a dielectric discontinuity, allowing the original wave to be reflected to the source.

The section of cliff scanned was chosen because of the abundance of channel bodies, in addition to ease of access. Laser scanning was completed on a clear, sunny day to avoid various problems, such as the increased reflectivity associated with scanning a wet outcrop and rain droplets. The LiDAR scan was performed at an average distance of approximately 100 m from the outcrop using a step-stare scan pattern with 12 mm point spacing. The point cloud is a collection of nearly 1.4 million points, following the deletion of extraneous points; all which are assigned an 8-bit intensity value between 0 and 255, in addition to a distinctive X (latitude), Y (longitude), and Z (elevation) value (i.e., each point has a unique coordinate).

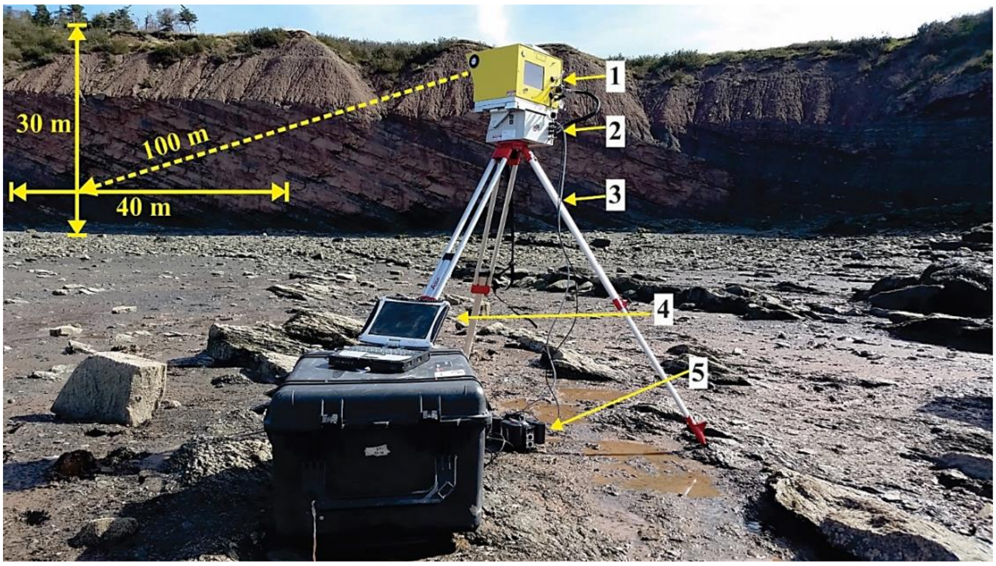

Fig. 4 A photograph of the Optech ILRIS-3D LiDAR scanner setup at Joggins, Nova Scotia [39]. Labelled in this photograph is the laser scanner (1), which was mounted atop the pan/tilt base (2), both of which were connected to a tripod (3). A ruggedized laptop computer (4) was used to adjust scanner settings and initiate the LiDAR scan. The LiDAR unit (1 and 2) is powered by a battery pack (5). The dipping strata of the Joggins Formation can be seen in the background. The distance between the LiDAR setup and the outcrop was approximately 100 m and is indicated by the dashed line.

The LiDAR system has numerous separate pieces that must be set up in a particular order. The procedure that was used for this scan is as follows:

a) setup and level the tripod;
b) mount the pan/tilt base to the levelled tripod;
c) mount the LiDAR scanner on top of the pan/tilt base;
d) measure the coordinates of the LiDAR setup using the RTK DGPS;
e) connect the LiDAR scanner to the pan/tilt base, the battery pack, and the ruggedized laptop computer using the required connectors and cables;
f) turn the system on and wait for boot up;
g) start the specialized software on the laptop computer and connect to the LiDAR scanner;
h) set the scan area using the software on the laptop computer and any other desired parameters;
i) initiate the scan and wait until complete.

2.2 Global Positioning System

The static terrestrial laser scanner was combined with a Real-Time Kinematic (RTK) Differential Global Positioning System (DGPS) (Fig. 5) to provide location data that was used to georeference the point cloud data set. The purpose of an RTK DGPS is to apply differential correction techniques that will improve the accuracy of the location data gathered by GPS receivers [38]. At the study area, the base station was set up over a water well cap on the oceanside (cliffside) of the Joggins Fossil Cliffs Centre, which has been previously surveyed to obtain its coordinates (UTM Zone 20T easting = 387,098.72; northing = 5,061,126.31; elevation = 26.45 m). The transmission antenna was positioned adjacent to the base station. Its purpose was to transmit the corrections made by the base station to the rover in real-time. The rover was mounted on an aluminum pole and was carried a maximum distance of ~ 600 m away from the base station/transmission antenna setup. The X, Y, and Z coordinates of each georeferencing target were recorded using the rover mounted RTK DGPS, following their placement inside the LiDAR scan survey area. This allows for LiDAR point cloud georeferencing to be finalized post-scan in the Basin and Reservoir Laboratory at Dalhousie University.

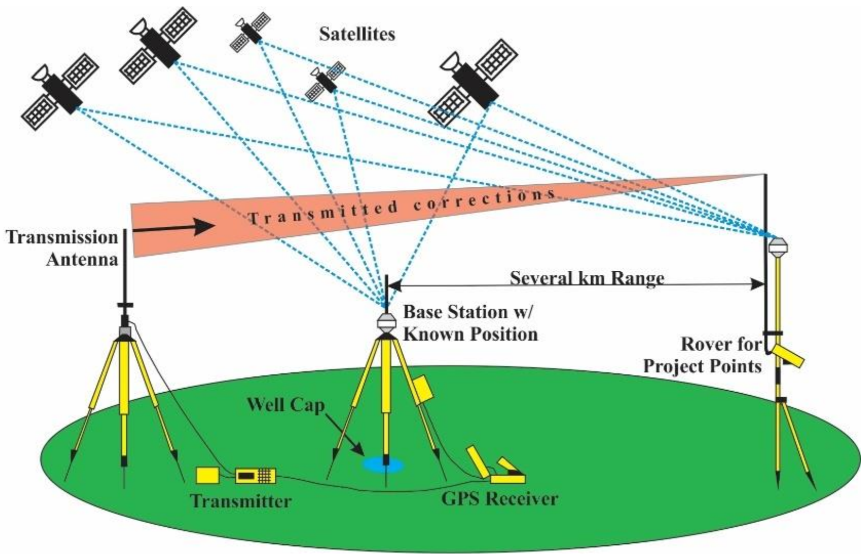

Fig. 5 Basic sketch of the global positioning system equipment used to collect location data for georeferencing a LiDAR data set post-scan [38]. The base station was erected over a water well cap with a known set of coordinates. The transmission antenna was placed adjacent to the base station. The rover was brought to the LiDAR survey area on the intertidal zone and utilized for measuring and recording the coordinates of the three LiDAR survey georeferencing targets.

The RTK DGPS also has numerous separate pieces that must be set up in a particular order. The procedure that was used for this scan is as follows:

a) the well cap of known coordinates was located on the backside (cliffside) of the Joggins Fossil Cliffs Centre, and the base station tripod was set up over this well cap and levelled by eye;
b) place the GPS receiver on the tripod and use the levelling screws to level;
c) setup the transmission antenna tripod directly adjacent to the base station and level by eye;
d) mount the transmission antenna on this tripod and extend to its maximum height;
e) connect the GPS receiver and transmission antenna to their respective power supplies as well as to each other using the required cables and connectors;
f) record the height of the base station above the well cap and use this value with the known coordinates of the well cap to determine the base stations location;
g) turn on all the various pieces of equipment, including the rover GPS and make sure both the base station and rover are synced with each other and both are receiving GPS data;
h) the rover GPS can now be taken to the intertidal zone and used for measuring the locations of the georeferencing targets and the LiDAR system setup.

2.3 Georeferencing Targets

Three georeferencing targets were incorporated into the LiDAR scan area to allow for the resulting point cloud to be georeferenced. A successful LiDAR scan must include at least three targets placed at varying X, Y, and Z locations so that triangulation can be performed, ensuring accuracy is maximized. The ideal placement for these three targets would be one placed at the top of the section, and the remaining two placed a distance apart on either side of the LiDAR scan area. However, due to logistics and accessibility, it was not feasible to place a target at the top of the cliff. Therefore, all three targets were placed at varying locations in the intertidal zone (Fig. 3B).

The targets are made of a 0.5 m by 0.5 m piece of plywood with an outer area covered in black, retro-reflective paint, and an inner circle (approximately 12 cm in diameter) that is white and non-reflective (Fig. 6A). Targets must be positioned such that the black outer area and white inner circle face the LiDAR unit and can be scanned by the LiDAR system (Fig. 6B). When the targets are scanned by the LiDAR unit, they return a distinctive intensity signature that when combined with the differential GPS readings of the centres of the non-reflective white inner circles, permits the scan to be georeferenced.

The setup of the three georeferencing targets is quick and straight-forward. The procedure that was used for this scan is as follows:

a) three locations a distance apart and at varying elevations within the scan field of view were selected;
b) a target was placed at each of the three locations, preferably resting against a larger rock for stability;
c) the RTK DGPS was used to measure the centre of each target.

Fig. 6 A) image of the LiDAR georeferencing targets that are placed at varying X, Y, and Z coordinates in front of the cliff face portion to be scanned [40]. B) image showing the placement of one of the georeferencing targets on the inter-tidal zone with the cliff and the Joggins Fossil Centre in the background [40].

2.4 Data

2.4.1 LiDAR/Target Setup Locations

The data consists of an easting, northing, and elevation value for each of the three targets and the LiDAR setup. The locations of the targets were determined by measuring the centres of each. The LiDAR setup location was determined by measuring the approximate centre of the glass lens housing the scanner.

2.4.2 LiDAR Point Cloud

The raw LiDAR data contains over 14.5 million points spread amongst four scan tasks. Some of these points are overlapping, and so can be eliminated. Before working with the raw LiDAR data, it is first necessary to use the parser software developed by the LiDAR manufacturer to export file formats that can be used.

2.5 Processing Procedure

The procedure for taking a raw, non-georeferenced LiDAR point cloud to a fully georeferenced point cloud is divided into four sections, listed here:

1) data preparation;
2) creation of point cloud/georeferencing target shapefiles;
3) point decimation;
4) point cloud adjustment.

2.5.1 Data Preparation

To prepare the raw LiDAR intensity data for eventual shapefile creation and subsequent adjustment, a simple workflow was applied. This ensured the point cloud data was in a compatible format for use with ArcGIS™ software.

Workflow

a) The raw .xyz files were opened using a simple text editor (e.g., Notepad) (Fig. 7A). A header line was added across the top corresponding to each column of data. The header line consists of an easting, northing, elevation, and intensity, each separated by one space only, which is the same format as the numerical data below the header.

b) The data was displayed with the easting, northing, elevation, and intensity values being separated by only one comma (Fig. 7B), using the *replace* option found in Notepad.

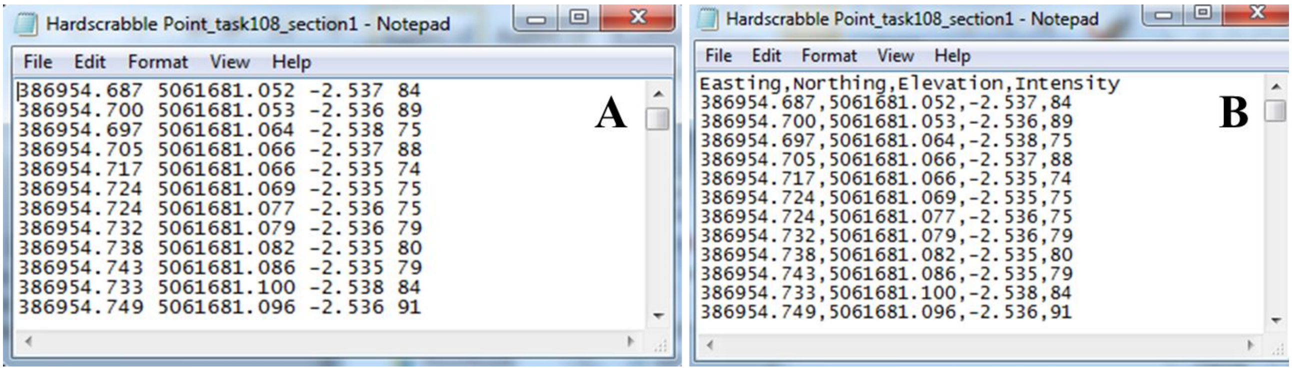

Fig. 7 A) Raw LiDAR intensity data displayed in Notepad. B) Raw LiDAR intensity data displayed in Notepad with the addition of a header line and all data separated by one comma.

2.5.2 Shapefile Creation

This section of the workflow utilizes ArcCatalog™, ArcScene™, and ArcMap™ for the creation of shapefiles. The produced shapefiles include the LiDAR point cloud shapefile, the false coordinate target locations, and the real coordinate target locations.

Workflow

a) In ArcCatalog™, use the *File* option from the menu toolbar to *Connect Folder*. Select the folder containing the text file created from the previous Data Preparation workflow. When the folder connects, the text document will be visible under the *Folder Connections* folder in the *Catalog Tree* pane.

b) Right-click the text document under *Folder Connections* and select *Create Feature Class* from *XY Table* (

c) Fig. 8A). For *Input Fields*, select the proper header description that describes the X Field, Y Field, and Z Field (e.g., easting, northing, and elevation) (Fig. 8B). Select the *Coordinate System of Input Coordinates* and choose the appropriate coordinate system. For the *Output — Specify output shapefile or feature class*, select the file folder symbol.

d) The *Saving Data* window will open. Navigate to the folder containing the text document. Be sure that the *Save as type* is selected as being a shapefile and select *Save* and *OK*. In ArcCatalog™, the newly created shapefile is now visible under *Fold Connections* (Fig. 9).

e) Choose a blank map in ArcScene™. Select the *File* drop-down menu and select *Add Data* and *Add Data*. The *Add Data* window will open. Double-click on the *Folder Connections* folder. Select the shapefile and choose *Add*.

f) When the shapefile opens, it will be a point cloud represented by a single colour (Fig. 10A). The easiest way to locate the targets in this point cloud is the application of a colour ramp (a set of different colours or shades that are used to represent a range of intensity values such that higher intensity values will display differently from lower intensity values). Using digital photographs of the scan area with the targets visible in the photographs will also help. Right-click on the shapefile and select *Properties*. Select the *Symbology* tab in the *Layer Properties* window and click on *Quantities* and *Graduated Colours*. In the *Fields* section, base the *Value* on Intensity. Select a *Colour Ramp* with a broad range of colours and set the *Classes* to at least 10. Click *Apply* and select the *OK* button. The point cloud will now be displayed with the colour based on intensity (Fig. 10B). It will now be possible to locate the targets in the scan.

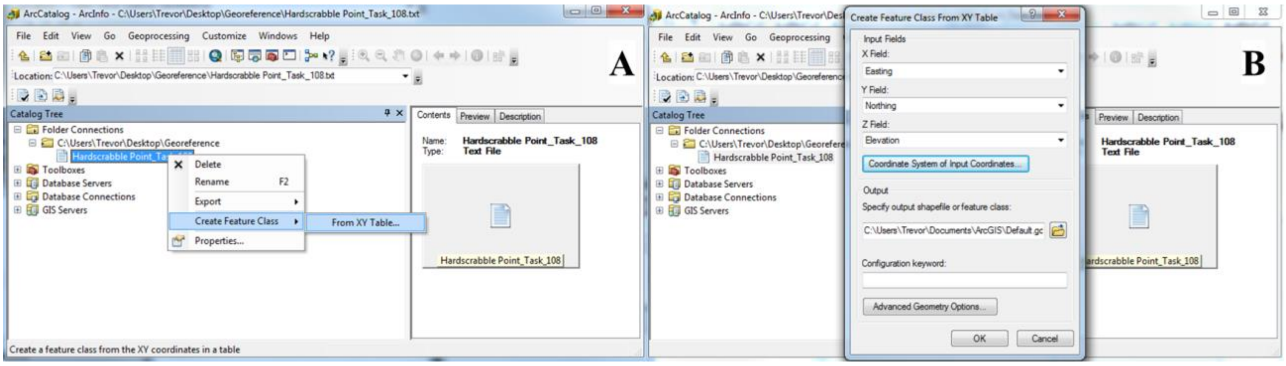

Fig. 8 **A) To create a shapefile from the text document, right-click on the text document, and expand *Create Feature Class*. Select *From XY Table*. B) A window will open called *Create Feature Class From XY Table*. For the *Input Fields*, select the proper header description that describes the *X Field*, *Y Field*, and *Z Field*. In this case, they are easting, northing, and elevation, respectively.**

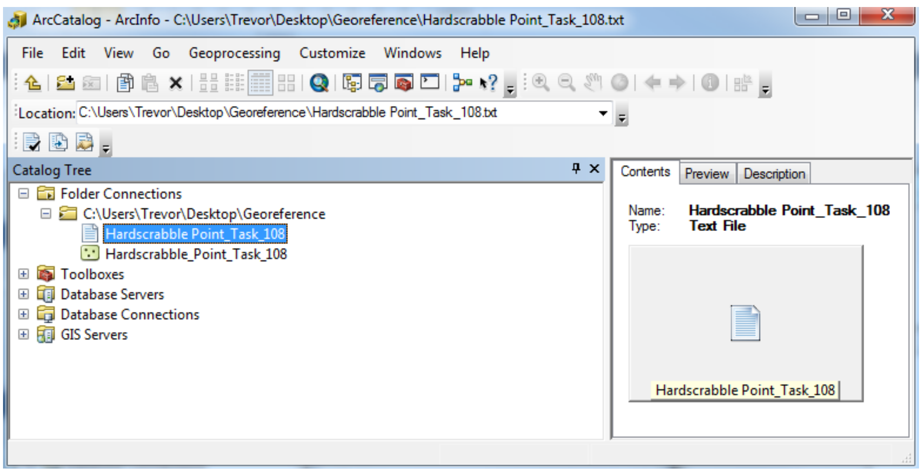

Fig. 9 **A screen capture from ArcCatalog™ showing the newly created shapefile under *Folder Connections* in the *Catalog Tree.***

g) Use the Bitmap images and JPEG images from the raw, unprocessed, and unparsed LiDAR data in addition to any photographs taken with a camera to help with locating the three georeferencing targets within the point cloud. The targets can be found by using various zoom/pan/tilt options in ArcScene™. The targets appear as a square of high-intensity points. In this case, the target can be seen resting against a boulder, as outlined by the black box (Fig. 11A). Using the *Identify* tool, click on the point that represents the centre of the target. Record the easting, northing, and elevation from the information that becomes available. Perform for the remaining two georeferencing targets (Fig. 11B).

h) With the three target locations recorded, which are the false locations, open Microsoft Excel and create a simple table like the one shown above (Fig. 11B). Save the file as a .csv (comma delimited) file within the Georeference named file that was created back at the start. Make another simple table like the one shown above, but this time input the correct coordinate locations as recorded by the differential global positioning system rover (Fig. 12). Save it the same way as the previous file.

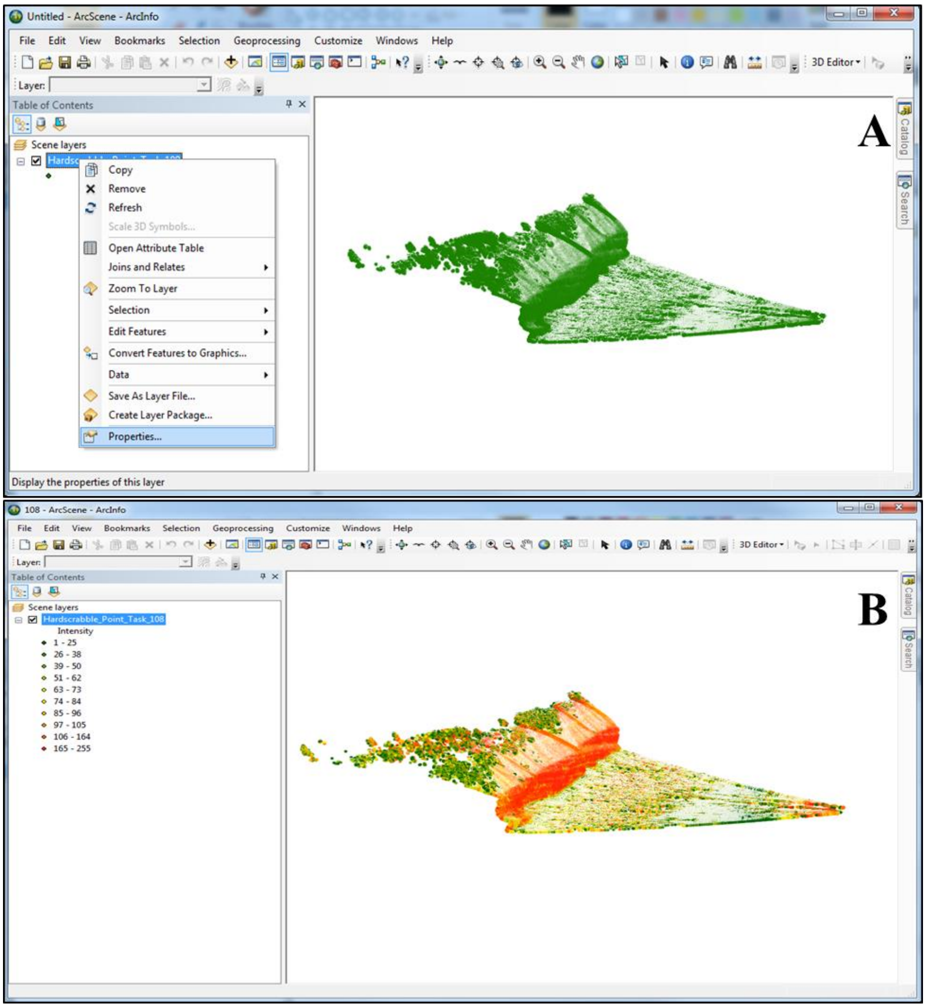

Fig. 10 A) Initially, the point cloud in ArcScene™ will be displayed in a single colour, which makes ground target locating very difficult. B) The same image as in A), but with a colour ramp based on intensity applied. Using this intensity-based colour scheme will make ground target locating easier.

i) In ArcCatalog™, refresh the folder to display the new .csv files. The previous steps for creating a shapefile can be applied to the false and real target location files to transform these files into shapefiles.

j) Select the *File* drop-down menu in ArcMap™. Choose *Add Data* and *Add Data*. When the window opens, select the three shapefiles, and click *Add* (Fig. 13A). Note the three points (boxed in green) in the right-hand corner; these are the real-world coordinates that we are trying to get the point cloud to georeference with (Fig. 13B). The other three points (circled in red) are the incorrect target locations (incorrect because the scan was performed without georeferencing); two of these points are concealed by the point cloud.

2.5.3 Point Decimation

To decrease the processing time and remove points not associated with the outcrop (the focus of concurrent research), many points can be deleted. The points represent objects/areas such as vegetation, infrastructure (e.g., houses, power lines, power poles, etc.), and the intertidal zone, which contains the highest number of erroneous points.

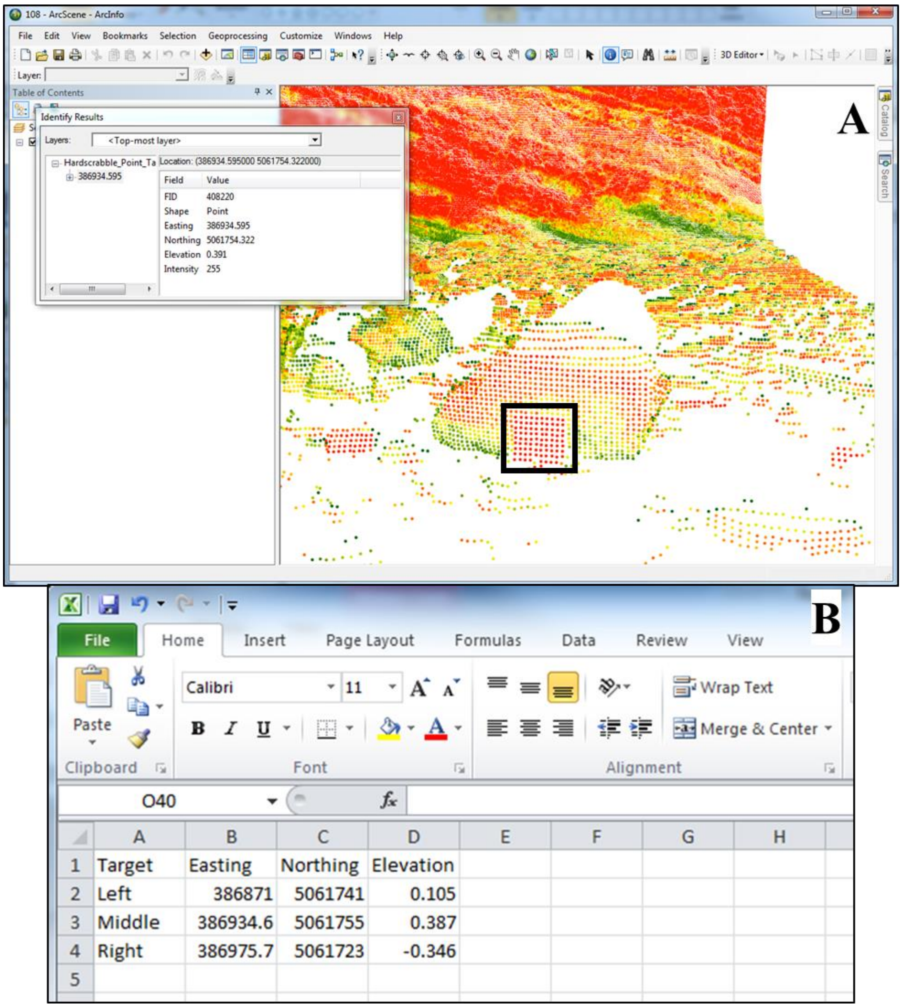

Fig. 11 A) The intensity-based point cloud showing one of the georeferencing targets within the black square. B) A simple table recording the false locations of the three georeferencing targets.

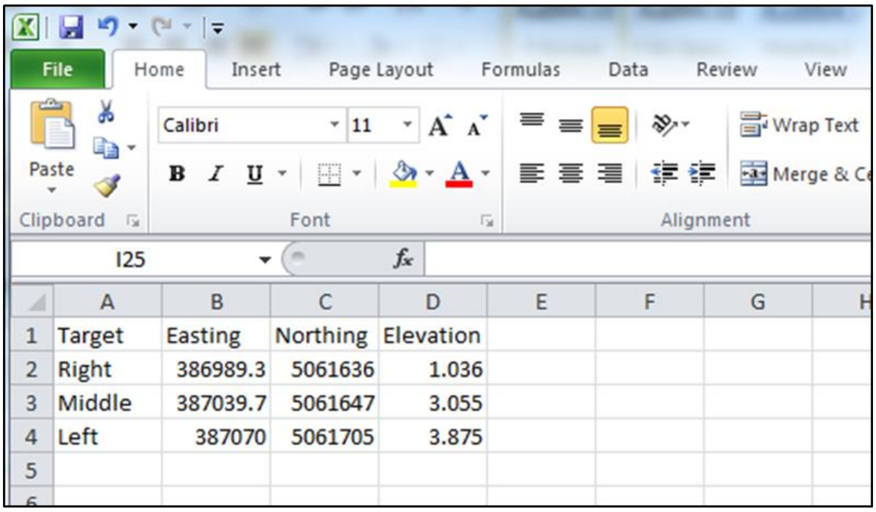

	A	B	C	D
1	Target	Easting	Northing	Elevation
2	Right	386989.3	5061636	1.036
3	Middle	387039.7	5061647	3.055
4	Left	387070	5061705	3.875

Fig. 12 A simple table containing the correct locations of the three georeferencing targets as measured by the RTK DGPS.

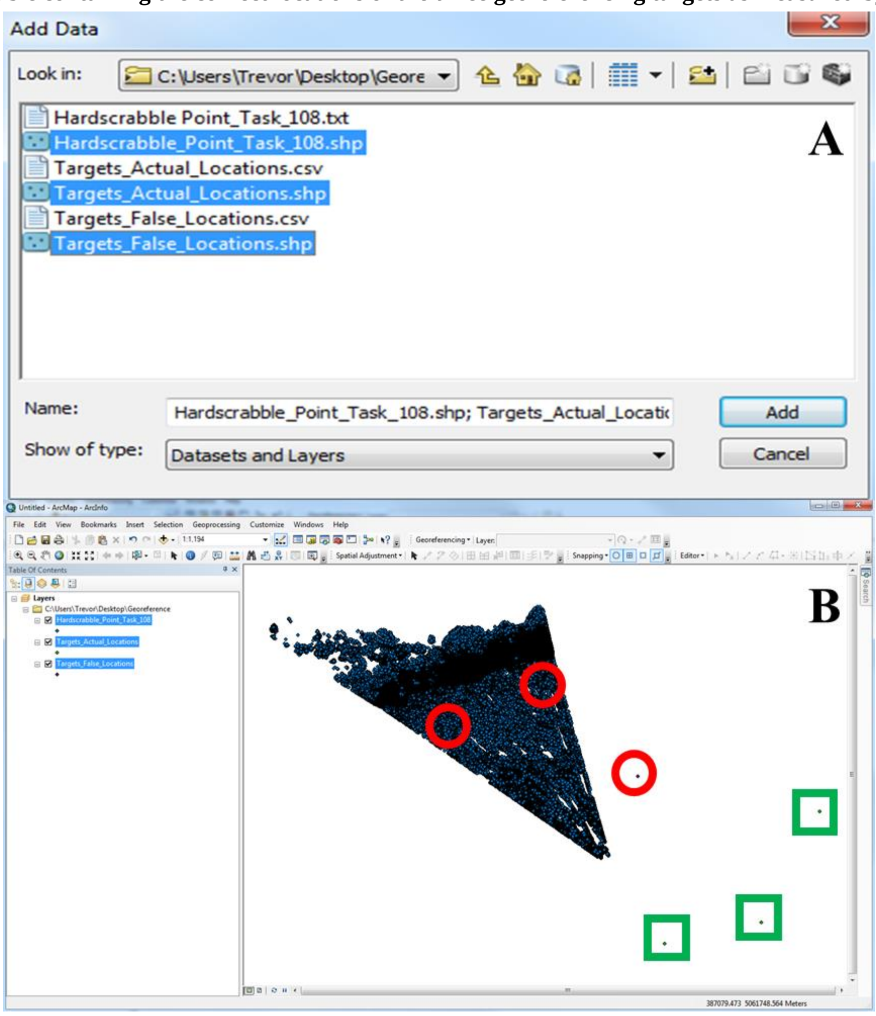

Fig. 13 A) An image showing the three shapefiles that have been created in this section B) An image that shows the three shapefiles displayed. The point cloud is visible as a triangular-shaped wedge. The false target locations are circled in red, and the real target locations are boxed in green.

Workflow

a) The two target locations shapefiles were turned off, leaving only the point cloud displayed. The *Select by Polygon* tool was used to batch select the points to delete (Fig. 14A). The chosen points were automatically highlighted in blue (Fig. 14B). The *Editor* drop-down menu was selected from the *Editor* toolbar, and the *Start Editing* option was chosen.

b) Right-click on the point cloud shapefile in the *Table of Contents* and select *Open Attribute Table* (Fig. 14B). At the bottom of the *Attribute Table*, choose to display only the highlighted points (Fig. 14B). Right-click on the left-hand edge of the *Attribute Table* and select *Delete Selected*. When finished, the records will be deleted. The *Attribute Table* can be closed.

c) Go back to the *Editor* drop-down menu and select *Save Edits*. The process was used several times to make the point cloud more manageable (Fig. 14C-D).

2.5.4 Point Cloud Adjustment

The previous workflows have been related to preparing the point cloud for georeferencing. The following outlines the steps to take a point cloud with a coordinate system based on the LiDAR setup to a geodetic coordinate system with every point displaying a unique X, Y, and Z value.

Workflow

a) The point cloud shapefile was turned off, leaving the two target location shapefiles visible (Fig. 15A). The *Start Editing* option was chosen from the *Editor* drop-down menu. Ensure that the *Spatial Adjustment* toolbar is activated and select the *Set Adjust Data* option (Fig. 15B). The *Choose Input for Adjustment* window will open. Select the *All features in these layers* option and un-check the correct target locations, since they do not need to be georeferenced (Fig. 15C).

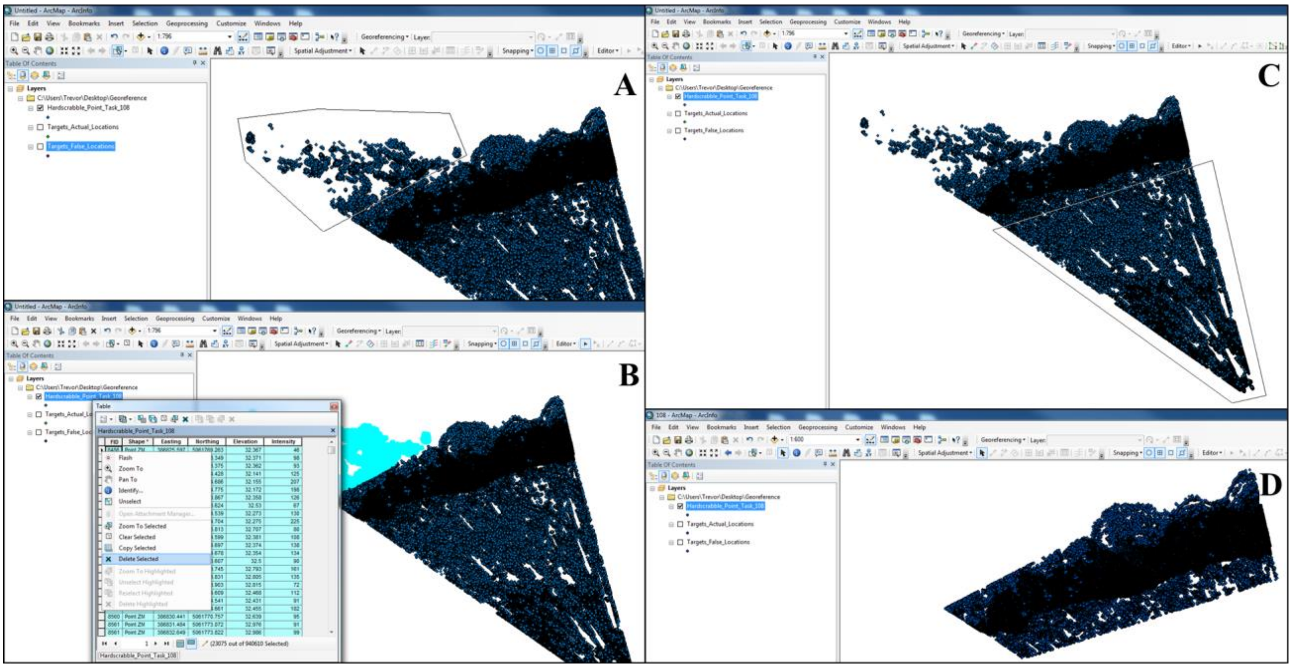

Fig. 14 A) The batch selection of non-useful points from the point cloud using a polygon. B) The non-useful points are highlighted in the attribute table and can be deleted as a group. C) The batch selection of the intertidal zone points using a polygon, which for this study is not useful. D) The final point cloud after the deletion of non-useful points.

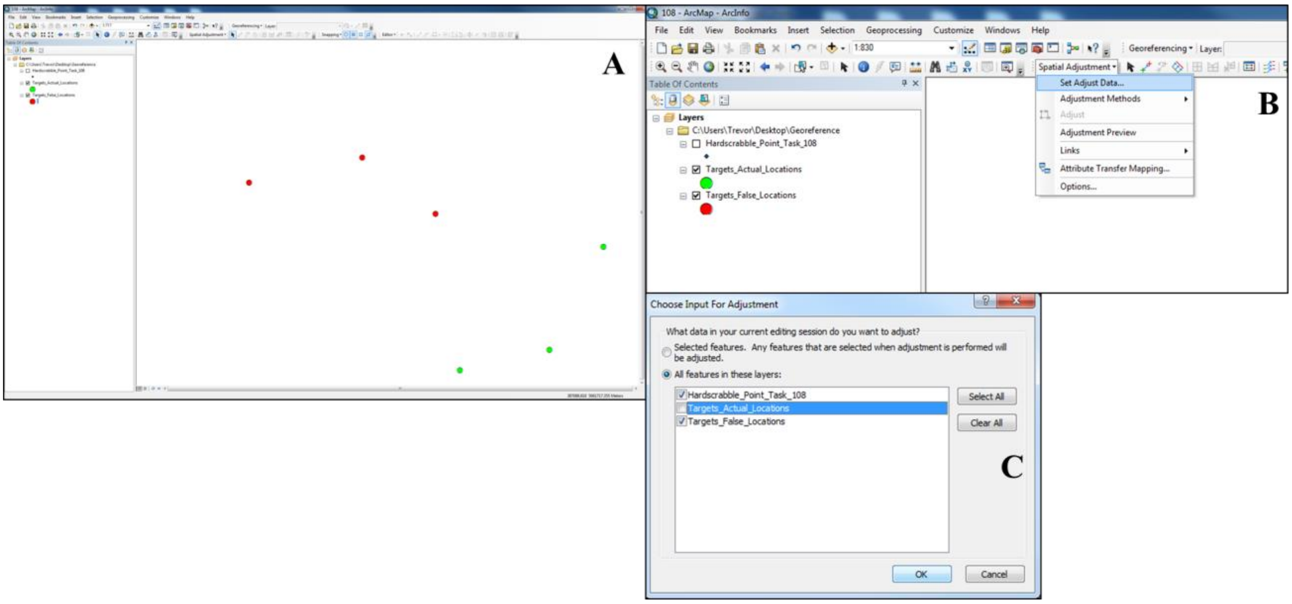

Fig. 15 A) The red points are the incorrect/false georeferencing target locations. The green points are the correct georeferencing target locations, as measured by the RTK DGPS. B) To adjust the incorrect georeferencing target locations and the point cloud, the *Set Adjust Data* must be selected from the *Spatial Adjustment* toolbar. C) To adjust the data, only choose the point cloud and the false georeferencing target locations.

b) In the *Spatial Adjustment* drop-down menu, the *Transformation-Affine* option from the *Adjustment Methods* was chosen (Fig. 16A). Select the *New Displacement Link* on the *Spatial Adjustment* toolbar (Fig. 16B). Select one of the false location points, which will snap to that point, then select the point that corresponds to the position where that point should be. This can be completed for the remaining two locations (Fig. 16C). Click on the *Spatial Adjustment* drop-down menu again and click on *Adjust*. When the adjustment is complete, select the *Editor* drop-down menu and choose *Save Edits*. The red points are not visible because they are overlain by the true target locations (green points). Turn the point cloud shapefile on (Fig. 17). The point cloud should now be georeferenced.

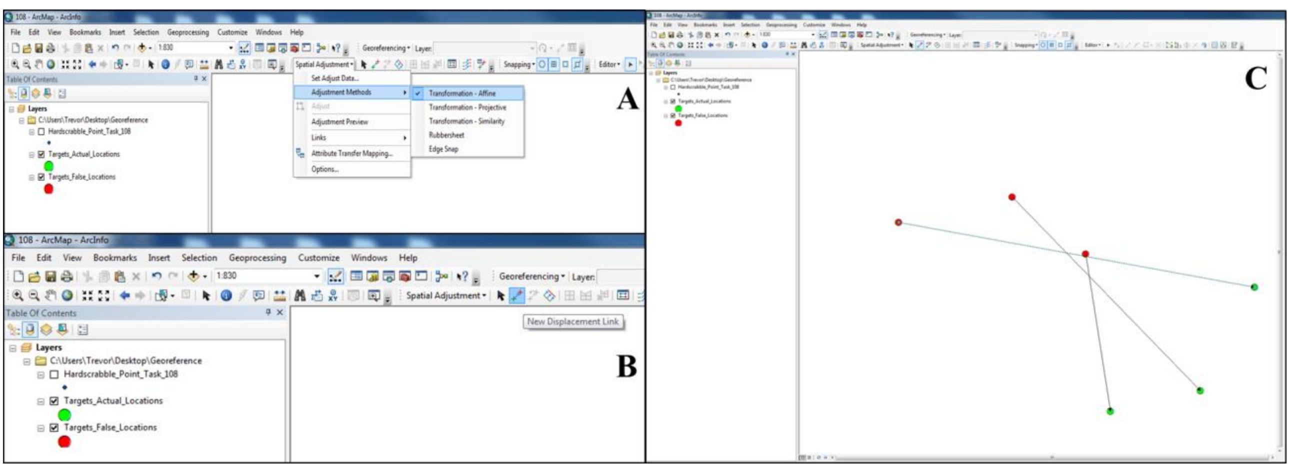

Fig. 16 A) The *Transformation-Affine* was chosen from the *Adjustment Methods* of the *Spatial Adjustment* tab. B) The location of the *New Displacement Link* highlighted in blue. C) The image shows how the points will be shifted.

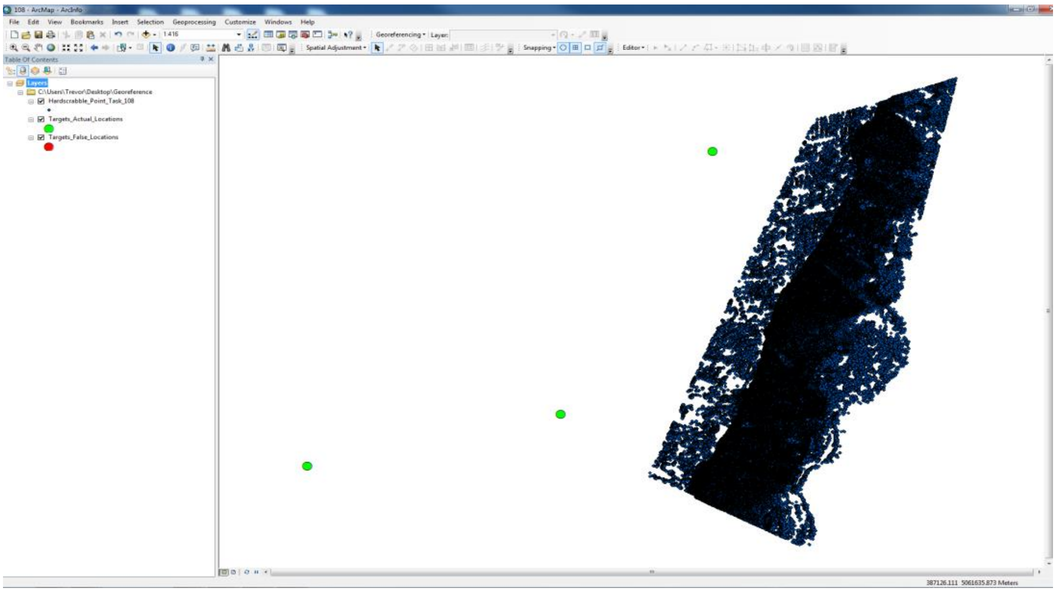

Fig. 17 An image showing the adjusted point cloud and false georeferencing target locations (which are overlain by the correct georeferencing target location points (green points).

c) With the point cloud shifted to its real-world coordinates, the *Attribute Table* can now be updated to display the new values for easting and northing. This is done by selecting the *Geoprocessing* drop-down menu and choosing *ArcToolbox*. In the *ArcToolbox* window that opens, expand the *Data Management Tools* option and expand the *Features* category. Select the *Add XY Coordinates* option. In the *Add XY Coordinates* window, click on the drop-down menu on the *Input Features* selection. Select the point cloud shapefile and click the *OK* button.

d) When the new coordinates have been written to the *Attribute Table* (Fig. 18), there should now be four new columns (Point_X, Point_Y, Point_Z, and Point_M). With the *Attribute Table* still open, it is now possible to export the data for use with other software. Click on the drop-down menu and select the *Export* option. When the *Export Data* window opens, click on the *Output* table file. Save the exported table to the folder created back at that start containing all the text files and shapefiles.

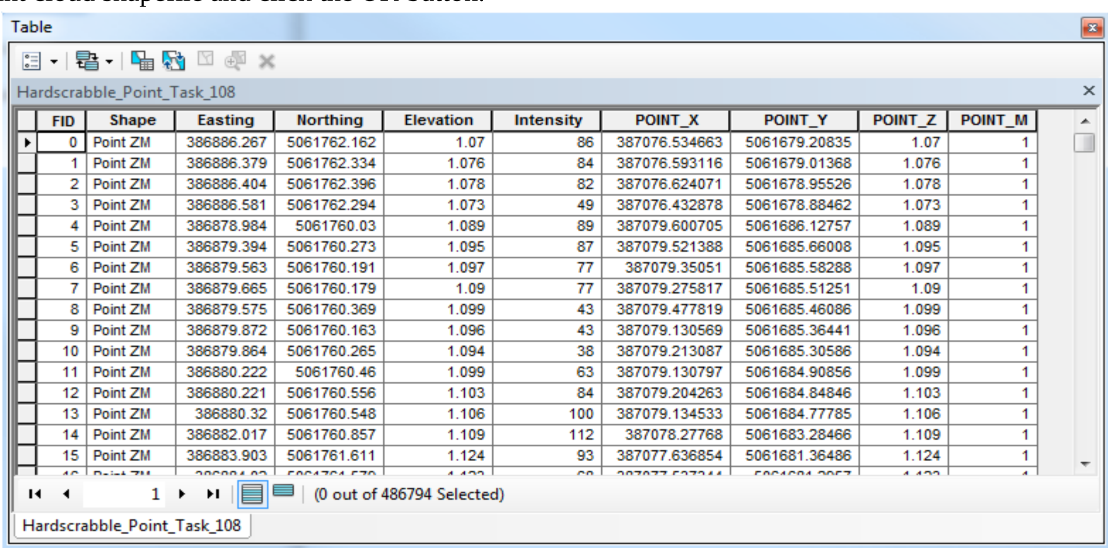

Table

Hardscrabble_Point_Task_108

FID	Shape	Easting	Northing	Elevation	Intensity	POINT_X	POINT_Y	POINT_Z	POINT_M
0	Point ZM	386886.267	5061762.162	1.07	86	387076.534663	5061679.20835	1.07	1
1	Point ZM	386886.379	5061762.334	1.076	84	387076.593116	5061679.01368	1.076	1
2	Point ZM	386886.404	5061762.396	1.078	82	387076.624071	5061678.95526	1.078	1
3	Point ZM	386886.581	5061762.294	1.073	49	387076.432878	5061678.88462	1.073	1
4	Point ZM	386878.984	5061760.03	1.089	89	387079.600705	5061686.12757	1.089	1
5	Point ZM	386879.394	5061760.273	1.095	87	387079.521388	5061685.66008	1.095	1
6	Point ZM	386879.563	5061760.191	1.097	77	387079.35051	5061685.58288	1.097	1
7	Point ZM	386879.665	5061760.179	1.09	77	387079.275817	5061685.51251	1.09	1
8	Point ZM	386879.575	5061760.369	1.099	43	387079.477819	5061685.46086	1.099	1
9	Point ZM	386879.872	5061760.163	1.096	43	387079.130569	5061685.36441	1.096	1
10	Point ZM	386879.864	5061760.265	1.094	38	387079.213087	5061685.30586	1.094	1
11	Point ZM	386880.222	5061760.46	1.099	63	387079.130797	5061684.90856	1.099	1
12	Point ZM	386880.221	5061760.556	1.103	84	387079.204263	5061684.84846	1.103	1
13	Point ZM	386880.32	5061760.548	1.106	100	387079.134533	5061684.77785	1.106	1
14	Point ZM	386882.017	5061760.857	1.109	112	387078.27768	5061683.28466	1.109	1
15	Point ZM	386883.903	5061761.611	1.124	93	387077.636854	5061681.36486	1.124	1

1 (0 out of 486794 Selected)

Hardscrabble_Point_Task_108

Fig. 18 The updated attribute table showing the four new columns.

It is now possible to open the data table in a data editing program like Microsoft Excel and delete all the irrelevant columns of data (keep new X, Y, and Z coordinates and the corresponding intensity values). For the example used in this paper, the relevant data were the updated eastings and northings, as well as the elevation and intensity. Also, of importance here is to realize that the point cloud used for the demonstration of this workflow is just one of four sections that make up the scanned area of the cliff face. The remaining three sections of the scan will also have to undergo a similar workflow to georeference them.

3. Results

Through the successful application of the procedure on the Joggins Formation LiDAR data set, the point cloud was significantly reduced from a cumbersome and processing-intensive, several million individual points to a manageable 1.4 million points. Initially, the point cloud contained millions of erroneous points representing the intertidal area, vegetation on the top of the cliff, and even some structures (houses, power lines, etc). Each of the points that comprise the point cloud has been fully georeferenced with unique easting, northing, and elevation values as a result of the combined usage of georeferencing targets and an RTK DGPS. Examples of the georeferenced point cloud are shown in Fig. 19, Fig. 20, and Fig. 21. This merged point cloud is now available for several studies relating to heterogeneity, coastal erosion, and ancient forest density, to name a few.

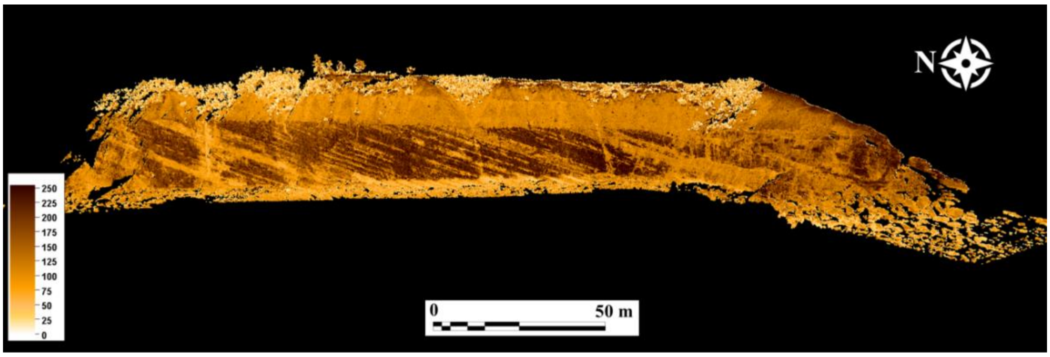

Fig. 19 Petrel E & P Software screen capture showing the point-decimated, fully georeferenced point cloud of the Joggins Formation cliff face. This image is a composition of the point cloud shown in the preceding workflow, along with the other three other scan sections merged. The colours are based on the LiDAR intensity with log sand, and shale colour ramp applied.

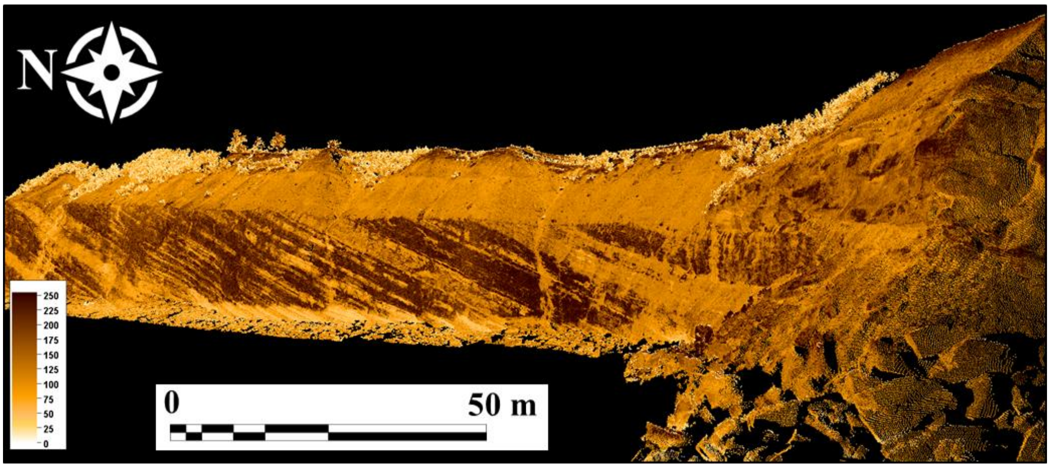

Fig. 20 Petrel E & P Software screen capture showing a view looking along the cliff face from the north at Coal Mine to the south.

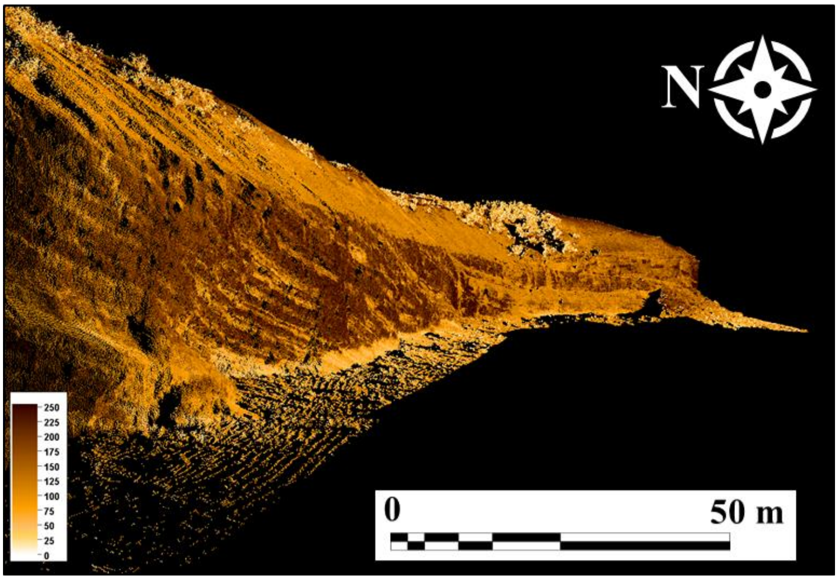

Fig. 21 Petrel E & P Software screen capture showing a view looking down the cliff face from the north to the south at Coal Mine Point. Notice that only a small number of points representing the intertidal area were left for reference.

With the successful completion of the workflow described herein, it is possible to have a fully georeferenced point cloud that displays the relevant points only with all erroneous points decimated and thus, lessening processing times and making interpretations easier. Initially, the point cloud contained a large number of intertidal points, vegetation on the top of the cliff, and even some structures (houses, power lines, etc). With all these points removed, the result is a cleaned point cloud that is ready for interpretation.

4. Discussion and Conclusions

The ideas presented in this paper detail one method of performing post-scan georeferencing analysis on a large geological outcrop section that has been scanned by a static terrestrial LiDAR scanner and paired with an RTK DGPS and control points. The application of commonly available software ensures that the methods can be applied consistently and efficiently with repeatable results. For LiDAR scans that must be performed in a relatively short amount of time (in this case due to tides), georeferencing post-scan has been shown to be a viable option. Post-scan georeferencing is advantageous when the laser scanner does not have built-in GPS capabilities or the built-in GPS capabilities of the laser scanner is not well known. Additionally, there could be potential errors in collecting GPS data directly during the scan, so using targets could serve as a backup. For multiple scans that will be eventually merged, highly accurate RTK DGPS data is required, which laser scanners do not have as a built-in option.

At Joggins and many other coastal cliffs that are subject to the rising and falling of tides, the most efficient use of time should be the collection of data. The time required to perform all the steps outlined in the workflow is rather short, depending on the processing capability of the computer workstation being utilized.

Accurately georeferenced data are particularly important for time series data sets in which the observation of real changes over a certain period is the goal. The uniqueness of Joggins Formation, with its fossilized, upright trees, offers researchers the possibility of studying paleo forest density using successive and georeferenced LiDAR scans taken over some time. Additionally, a georeferenced point cloud can be easily integrated with other data gathering techniques, such as a ground-penetrating radar survey, for example.

Acknowledgments

We want to thank Dr. Lawrence Plug of the Dalhousie University Department of Earth Sciences for allowing the use of the real-time kinematic differential global positioning system equipment. We also want to thank Johnathan Thibodeau for his field assistance and for constructing the georeferencing targets. I would like to thank the two anonymous reviewers for assessing this manuscript. Finally, the members of the Dalhousie University Basin and Reservoir Laboratory are acknowledged for their help with the fieldwork.

References

[1] D. Minisini, M. Wang, S. C. Bergman and C. Aiken, Geological data extraction from lidar 3-D photorealistic models: A case study in an organic-rich mudstone, Eagle Ford Formation, Texas, *Geosphere* 10 (2014) 610-626.

[2] A. Rotevatn, A. Torabi, H. Fossen and A. Braathen, Slipped deformation bands: A new type of cataclastic deformation bands in Western Sinai, Suez rift, Egypt, *Journal of Structural Geology* 30 (2008) 1317-1331, doi: 10.1016/j.jsg.2008.06.010.

[3] A. Rotevatn, S. J. Buckley, J. A. Howell and H. Fossen, Overlapping faults and their effect on fluid flow in different reservoir types: A LIDAR-based outcrop modeling and flow simulation study, *AA PG Bulletin* 93 (2009) 407-427.

[4] H. Sahoo and N. D. Gani, Creating three-dimensional channel bodies in LiDAR-integrated outcrop characterization: A new approach for improved stratigraphic analysis, *Geosphere* 11 (2015) 777-785.

[5] C. Beumier, Vehicle speed estimation from two images for LIDAR second assessment, *VISAPP* (2012) (2) 381-386.

[6] M. Griggs and C. B. Ludwig, Legal aspects of remote sensing and air enforcement, *Journal of the Air Pollution Control Association* 28 (1978) 119-122.

[7] B. T. Wu, P. C. Li, J. H. Chen, Y. J. Li and Y. C. Fan, 3D environment detection using multi-view color images and LiDAR point clouds, in: *2018 IEEE International Conference on Consumer Electronics-Taiwan (ICCE-TW)*, IEEE, 2018, pp. 1-2.

[8] S. Lim, C. A. Thatcher, J. C. Brock, D. R. Kimbrow, J. J. Danielson and B. J. Reynolds, Accuracy assessment of a mobile terrestrial lidar survey at Padre Island National Seashore, *International Journal of Remote Sensing* 34 (2013) 6355-6366, doi: 10.1080/01431161.2013.800658.

[9] R. Xharde, B. F. Long and D. L. Forbes, Accuracy and limitations of airborne LiDAR surveys in coastal environments, in: *International Geoscience and Remote Sensing Symposium*, Denver, CO, 2006, pp. 2412-2415.

[10] S. Kwon, J. W. Park, D. Moon, S. Jung and H. Park, Smart merging method for hybrid point cloud data using UAV and LIDAR in earthwork construction, *Procedia Engineering*, 196 (2017) 21-28.

[11] N. Puri and Y. Turkan, Bridge construction progress monitoring using lidar and 4D design models, *Automation in Construction* 109 (2020) 102961.

[12] S. Yoon, Q. Wang and H. Sohn, Optimal Placement of Precast Bridge Deck Slabs with respect to Precast Girders using LiDAR, in: *ISARC: Proceedings of the International Symposium on Automation and Robotics in Construction*, Vilnius Gediminas Technical University, Department of Construction Economics, 2017, Vol. 34.

[13] A. Habib, A. Jarvis, A. Kersting and Y. Alghamdi, Comparative analysis of georeferencing procedures using various sources of control data, in: *21st ISPRS Proceedings*, 2008, pp. 3-11.

[14] J. Llorens, E. Gil, J. Llop and M. Queraltó, Georeferenced LiDAR 3D vine plantation map generation, *Sensors* 11 (2011) 6237-6256.

[15] A. Mohamed and B. Wilkinson, Direct georeferencing of stationary LiDAR, *Remote Sensing* 1 (2009) 1321-1337.

[16] M. J. Olsen, E. Johnstone, N. Driscoll, S. A. Ashford and F. Kuester, Terrestrial laser scanning of extended cliff sections in dynamic environments: Parameter analysis, *Journal of Surveying Engineering* 135 (2009) 161-169.

[17] M. J. Olsen, Putting the pieces together: Laser scan geo-referencing, *LiDAR Magazine* 1 (2011).

[18] S. Schuhmacher and J. Böhm, Georeferencing of terrestrial laser scanner data for applications in architectural modeling, in: *Proceedings of the ISPRS Working Group V/4 Workshop 3DARCH "Virtual Reconstruction and Visualization of Complex Architectures"*, Mestre-Venice, Italy, 22-24 August, 2005, pp. 1-7.

[19] B. E. Wilkinson, A. H. Mohamed, B. A. Dewitt and G. H. Seedahmed, A novel approach to terrestrial LiDAR georeferencing, *Photogrammetric Engineering & Remote Sensing* 76 (2010) 683-690.

[20] Y. Zhang and X. Shen, Direct georeferencing of airborne LiDAR data in national coordinates, *ISPRS Journal of Photogrammetry and Remote Sensing* 84 (2013) 43-51.

[21] J. A. Bellian, C. Kerans and D. C. Jennette, Digital outcrop models: applications of terrestrial scanning lidar technology in stratigraphic modeling, *Journal of Sedimentary Research* 75 (2005) 166-176.

[22] A. M. Baldridge, S. J. Hook, C. I. Grove and G. Rivera, The ASTER spectral library version 2.0, *Remote Sensing of Environment* 113 (2009) 711-715, doi:

10.1016/j.rse.2008.11.007.

[23] D. Burton, D. B. Dunlap, L. J. Wood and P. P. Flaig, Lidar intensity as a remote sensor of rock properties, *Journal of Sedimentary Research* 81 (2011) 339-347, doi: 10.2110/jsr.2011.31.

[24] C. Wong, Lidar survey of the Joggins Formation in the Coal Mine Point section, Cumberland Basin (Nova Scotia, Canada). Department of Earth Sciences, Dalhousie University, Halifax, Nova Scotia, 2014.

[25] M. J. Olsen, E. Johnstone, F. Kuester, N. Driscoll and S. A. Ashford, New automated point-cloud alignment for ground-based light detection and ranging data of long coastal sections, *Journal of Surveying Engineering* 137 (2011) 14-25.

[26] M. Grey and Z. V. Finkel, The Joggins Fossil Cliffs UNESCO World Heritage site: A review of recent research, *Atlantic Geology* 47 (2011) 185-200, doi: 10.4138/atlgeol.2011.009.

[27] UNESCO, World Heritage List — Joggins Fossil Cliffs, 2008, accessed on 6 Sep. 2018, available online at: http://www.whc.unesco.org/en/list/1285/.

[28] H. J. Falcon-Lang, Earliest history of coal mining and grindstone quarrying at Joggins, Nova Scotia, and its implications for the meaning of the place name "Joggins", *Atlantic Geology* 45 (2009) 1-20, doi: 10.4138/atlgeol.2009.001.

[29] J. H. Calder and J. Boon, Joggins Fossil Cliffs: Property nominated for inscription on the world heritage list, Nova Scotia Department of Natural Resources, Mineral Resources Branch, Halifax, NS, Open File Map ME 2007-2001, 2007.

[30] Nova Scotia Department of Natural Resources, Aerial Photography - 2005 Colour Photographs, 2005.

[31] Optech Incorporated, *ILRIS-3D Operation Manual*, 2006.

[32] J. A. Bellian, R. Beck and C. Kerans, Analysis of hyperspectral and lidar data: Remote optical mineralogy and fracture identification, *Geosphere* 3 (2007) 491-500.

[33] A. Grechishnikova, Integrated application of a high-resolution LIDAR outcrop survey of an unconventional Niobrara Reservoir, Denver Basin, Colorado, *First Break* 34 (2016) 65-71.

[34] J. Moore, A. Taylor, C. Johnson, B. D. Ritts and R. Archer, Facies analysis, reservoir characterization, and LIDAR modeling of an Eocene lacustrine delta, Green River Formation, southwest Uinta Basin, Utah, 2012.

[35] F. Rarity, X. Van Lanen, D. Hodgetts, R. Gawthorpe, P. Wilson, I. Fabuel-Perez and J. Redfern, LiDAR-based digital outcrops for sedimentological analysis: workflows and techniques, *Geological Society* 387 (2014) 153-183.

[36] N. A. Siddiqui, M. Ramkumar, A. H. A. Rahman, M. J. Mathew, M. Santosh, C. W. Sum and D. Menier, High resolution facies architecture and digital outcrop modeling of the Sandakan formation sandstone reservoir, Borneo: Implications for reservoir characterization and flow simulation, Geoscience Frontiers (2018).

[37] Q. Zeng, W. Lu, R. Zhang, J. Zhao, P. Ren and B. Wang, LIDAR-based fracture characterization and controlling factors analysis: An outcrop case from Kuqa Depression, NW China, *Journal of Petroleum Science and Engineering* 161 (2018) 445-457.

[38] J. Van Sickle, *GPS for Land Surveyors*, CRC Press, 2015.

[39] T. B. Kelly and G. D. Wach, Analysis of factors influencing the interpretation of a digitally examined fluvial meanderbelt system: Joggins Formation, Nova Scotia, *Canadian Journal of Earth Sciences* 57 (2020) 524-541, doi: 10.1139/cjes-2018-0263.

[40] C. Rafuse and G. Wach, Reservoir architecture of meanderbelt systems and vegetation density in the Carboniferous using LiDAR imagery, Earth Sciences, Dalhousie University, Halifax, NS, 2011.